Received: 09.09.2022; Revised: 14.12.2022; Accepted: 22.02.2023

UKRAINIAN JOURNAL OF FOREST AND WOOD SCIENCE

Journal homepage: https://forestscience.com.ua/en
Ukrainian Journal of Forest and Wood Science, 14(1)

UDC 630*5(528)
DOI: 10.31548/forest/1.2023.72

Land cover classification and urbanization monitoring using Landsat data: A case study in Changsha city, Hunan province, China

Mykola Kutia*
PhD, Senior Lecturer
Bangor College China, Bangor University
410004, 498 Shaoshan Rd., Changsha, China
https://orcid.org/0000-0001-9996-2653

Jiawei Li
MSc Student
University of Southampton
SO17 1BJ, Southampton, United Kingdom
https://orcid.org/0000-0002-3481-2942

Arbi Sarkissian
PhD, Lecturer
Lancaster University
LA1 4YW, Lancaster, United Kingdom
https://orcid.org/0000-0003-4094-0884

Tim Pagella
PhD, Senior Lecturer
Bangor University
LL57 2DG, Bangor, Gwynedd, United Kingdom
https://orcid.org/0000-0001-5926-9299

Abstract. The United Nations predicts that by 2050, 64.1% of the developing world and 85.9% of the developed world will be urbanized. This has resulted in a rapid change in land use and land cover types in the areas surrounding cities in all countries, particularly in China, which determines the relevance of this article. The aim of the study was to evaluate the dynamics of land cover change in Changsha City, Hunan Province, China, between 2005 and 2020, using Landsat time series satellite images and the Random Forest classification algorithm. The data acquisition, pre-processing, and analysis were conducted on the Google Earth Engine (GEE) publicly available online platform.

Suggested Citation:

Kutia, M., Li, J., Sarkissian, A., & Pagella, T. (2023). Land cover classification and urbanization monitoring using Landsat data: A case study in Changsha city, Hunan province, China. *Ukrainian Journal of Forest and Wood Science*, 14(1), 72-91. doi: 10.31548/forest/1.2023.72.

*Corresponding author

Land cover thematic continuous raster maps were produced using ESRI ArcGIS 10.5.1 software. The overall classification accuracy was obtained by more than 83% for every produced map and the Kappa coefficient was 0.84 and higher, which approves the reliable classification results that are close to similar recent studies in terms of obtained accuracy. The study shows that from 2005 to 2020, the area of settlement in Changsha City, China, increased significantly, with an exponential increase in urban area from 3.23% to 15.95%. The proportion of forest cover gradually decreased from 2005 to 2015 but increased from 2015 to 2020. Cropland was the second most dominant land cover type, with a peak of almost 50% in 2010. Water bodies remained stable at around 3%. The proportion of open soil and bare land cover fluctuated between 180 and 400 km2 (1.5-3%). The study suggests that the offered monitoring approach provides reliable results, and the research findings can be used for sustainable urban planning and management, as well as conservation and development initiatives. The remote sensing data and advanced GIS technologies can provide decision-makers with the accurate data to ensure sustainable development in this area

Keywords: accuracy estimation; Random Forest algorithm; satellite imagery; overall accuracy; urban expansion

Introduction

As the capital city of Hunan province and one of the most important cities in central China, Changsha has expanded at an astounding speed in recent years (Zhou & He, 2007). According to S. Su *et al.* (2011) urban expansion not only facilitates people's life, but also causes a series of environmental, transportation and climate problems; thus, affecting agriculture (Seto *et al.*, 2000), water resources and natural environment (Zhang *et al.*, 2010), even accelerating the spread of diseases (Miao & Wu, 2016) and bringing multiple challenges to urban planning and management (Batty, 2008). Y. Liu *et al.* (2021) analysed the urban expansion dynamics of the Xiaonan District in Hubei Province, China using Landsat satellite imagery and landscape metrics. The results showed that urban areas expanded rapidly during the period 1990-2020, and the expansion was accompanied by significant changes in landscape pattern and fragmentation. The study highlighted the importance of considering both the extent and pattern of urban expansion in urban planning and management.

Based on remote sensing (RS), as a non-contact technology, LULC thematic surface cover maps can be produced, including woodland, water, build-up areas and other categories. P. Corona (2010) proved that LULC distribution data can be widely applied in assessing environment and monitoring work, such as Climate change, food security, agricultural statistics (Kolotii *et al.*, 2015; Ma *et al.*, 2015) and so on. Reliable urban LULC maps can be used in more accurate urbanization process assessment and area calculation on a regional scale, which guides more effective urban planning policies. At present, various satellite systems provide objective, high spatial resolution data on a regular basis.

However, D.P. Roy *et al.* (2014) described in their work that public available medium resolution Landsat imagery, because of their continuity and long observation history, allows to regularly evaluate LULC changes in large areas. J. Friedmann (2003) concluded that under the background of the rise of Central China, the study on the expansion mechanisms of urban construction land in Changsha city can not only

provide a reference for other cities of Central China to achieve sustainable development and formulate relevant policies, but also provide a case study to reveal trends of urban expansion in China. Therefore, it is crucial to study the scope and speed of urban expansion, as well as the dynamic changes of land use and land cover (LULC) in the city.

Using time series of Landsat imagery received during one calendar year or longer, various tasks of the thematic classification can be solved. Thus, the annual set of images can provide information about LULC changes of study area. Given the large number of variables (bands and band ratios) required, non-parametric methods of classification provide reliable results without the assumption that the data must have normal distribution character.

The purpose was to analyse based on multispectral satellite imagery and random forest method, the LULC distribution map of Changsha over recent 15 years period, as well as the spatial and temporal characteristics of the expansion of construction land. Based on the above mentioned, the tasks for this study were: to perform pixel based classification of Landsat time-series image composites and produce Land cover raster maps for years 2005, 2010, 2015, and 2020 within Changsha city administrative unit using Random Forest supervised classification algorithm; to determine the relationship between urban growth, agriculture and forest cover dynamics; to assess the accuracy of the obtained mapping materials and compare them with other sources and similar studies.

Literature Review

China is the country that started urbanization the earliest, develop urbanization slowly until decades ago and develop fast recently. J. Friedmann (2011) evaluates the rapid urbanization process of China as "urbanizing at breakneck speed". The number of cities has increased from 122 (in year 1950) to 674 now and the number of towns has increased from 2176 (in 1978) (Martinez *et al.*, 2017) to 16702 now.

X. Chen *et al.* (2015) described the rapid urbanization process not only accumulates national wealth, but also caused some land use, environmental and social problems in China. On social issues, over-speed urbanization has led to a phenomenon that the rural floating population only participates in the secondary labour of cities but can't really integrate into the culture, society and system of urban area, which is called "semi-urbanization", a sub-health state of the cities. On environmental issues, M. Jin *et al.* (2005), J. Zhang *et al.* (2010) found that environmental degradation such as deforestation, traffic pollution, microclimate change and so on were unavoidable in the process of urbanization. On land use issues, ever-increasing urban area has spread at an astounding rate in recent decade, however, at cropland's expense. From 1949 to 1980, almost 14667 km^2 decreased during the 30 years. H. Li *et al.* (2015) researched that during the next 15 years (from 1981 to 1995), the net loss of arable land was more than 54000 km^2.

The reasonable use of urban land can limit the over-speed of urban expansion and negative impacts. In order to make China's urbanization process in an appropriate way, people need to start with the driving force of urbanization and regulate it. L. Feng *et al.* (2017) has referred to numerous literatures and selected 4 indicators as independent variables. Through the calculation of multiple linear regression model, it is found that market force (market) is the most important driving force, followed by endogenous force (grassroots government or farmers), administrative force (government's capital policy) and extroverted force (foreign capital) (Chaolin *et al.*, 2012). Y. Yan *et al*. (2020) used Landsat images to extract land cover information and analyse spatiotemporal patterns

of urban expansion in the Pearl River Delta urban agglomeration in China. This study reveals that economic development, transportation infrastructure, and population growth were the main drivers of urban expansion in the area.

The fact that the endogenous force is greater than the exogenous force indicates that China's urbanization is mainly dominated by internal factors although the world has entered the global era (Luo & Yan, 2018). Hence, it is important to know the land use and land cover change (LULC) to support the government to adopt suitable land use and distribution policies.

Land use shows how people use landscape, whether for development, conservation or mixed function (Lambin *et al.*, 2001). Land cover means that the undulating land surface (including the soil layer) covered with vegetation, snow, glaciers, or water (Lin *et al.*, 2018). Land cover has also been defined that vegetation or other features overlay on the earth surface (Song & Deng, 2017).

X. Lambin *et al*. (2001) stated that the remote sensing image classification is an important content of image analysis, which is used to estimate the area range and spatial distribution of various types of land cover, even widely applied in tropical deforestation, rangeland modifications, agricultural intensification etc. It uses computers and software to analyse the spatial information and spectral information of different objects in the image, select features, then divide the feature space into non-overlapping subspaces and finally assign each pixel in the image to the subspace (Ayanu *et al.*, 2015).

N. Puletti *et al*. (2014) found that according to the classified data of training samples are known or not, image classification algorithms can be divided into supervised classification and unsupervised classification. The Unsupervised classification has no pre-confirmed categories so that training data cannot be established. The classification is based on the difference of spectral features or other features of different images and ground objects in the feature space and the clustering statistical analysis of images can be carried out by computers.

The supervised classification of remote sensing imagery is a process which includes an extraction from training samples of each class from the known training field, and classify each pixel point in the image into each given class by selecting characteristic variables, determining discriminant function or discriminant. It refers to the process that identified pixels (pixel in the training area) recognize and analyse unrecognized pixels. In this classification, a certain number of each class on the image is selected, and based on them, the statistics or other information of each training sample area will be calculated by computers which was discussed by Y. Ayanu *et al*. (2015). Specifically, each pixel is compared with the training sample.

There are many supervised classification algorithms (classifiers). Nowadays, most commonly used non-parametric algorithms based on machine learning principles such as Random Forest, Support Vector Machine, Classification and Regression Trees, Neural Networks etc. Random forest (RF) was firstly input by L. Breiman (2001) in 2001. It is a powerful image classification technology with anti-overfitting ability, which can process segmented images and other auxiliary raster data sets. The principle and procedure are described following: The total data set consists of all training data, 2/3 training samples of it are extracted as training set. Next, the training set is put back and then the next random sampling is conducted (Simple random sampling with replacement) until the "N" time, to obtain N training sets (decision trees), which is called Bagging principle in the research conducted by V. Eisavi *et al*. (2015). We assume that these N training sets contain M feature variables totally (training feature files). Then m feature variables are extracted

from each decision tree (m<M) and every result is finished. The result with the highest number of repeats (voting method) from N results becomes the final prediction result. In each sample, about 1/3 training samples which are not selected, and called as out-of-bag (OOB). OOB can be used to estimate the internal error and generate OOB error, which is used to predict the accuracy of classification (He *et al.*, 2016). For the successful application of RF classifier, two parameters must be set: the number of classification trees (ntree) and the number of input variables used at each node (mtry).

From the first RS satellite Landsat 1 which was launched in 1972, in past decades, with the improvement of Remote sensing (RS) and Geographic Information System (GIS) technology, many advanced classification methods, land use and land cover change maps have been produced based on Landsat imagery analysis provided by R. Welch *et al.* (1975). M. Kutia *et al.* (2018) in their study utilised the Google earth engine (GEE) as a cloud-based platform for scientific analysis and free access for satellite imageries. It stores decades-old images and scientific datasets (at petabyte-scale). In 2008, with the free availability of the Landsat series, Google archived all datasets and linked them to the cloud computing engine, for acquisition of open-source data according to O. Firpi (2016). The GEE computing engine provides both JavaScript and Python application programming interfaces (apis) that is allowed to easily develop algorithms that work in parallel on a Google data computer facility.

Materials and Methods

Study area. Changsha is the capital and most populous city of Hunan province (27°51′-28°41′N, 111°53′-114°15′E) (Fig. 1) in the south-central part of the People's Republic of China, covering approximately 11 819 km^2 (about 230 kilometers long from east to west and 88 kilometers wide from south to north). Also, it is an important central city in the middle reaches of the Yangtze River. It is about 118-127 days in summer, 117-122 days in winter, and 61-64 days in spring and 59-69 days in autumn (Zhou & He, 2007). Changsha has a subtropical monsoon climate. The annual average high temperature is 22.0°C and the low is 13.3°C. The annual rainfall is around 1615.4 mm. The average annual air pressure is 101 thousand PPA. The average annual sunshine period is 1640-1700 hours and the relative humidity is 81% (Yao *et al.*, 2018).

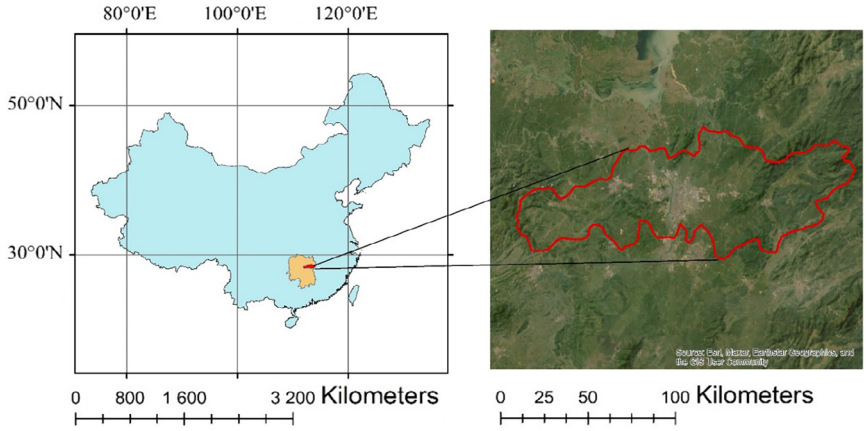

Figure 1. The location of Changsha City in Hunan Province, P.R. of China

Source: Esri, Maxar, Earthstar Geographics, and the GIS User Community

It is surrounded by mountains which are relatively high at both the northeast and northwest; while the central part is gentle, therefore looking likes a saddleback. Xiangjiang River runs through the central part from the south to the north, and the southern part is hilly and undulating, in contrast, the northern part is flat and open (Tse-Tung, 2017). Red soil and paddy soil is main soil in Changsha, accounting for 70% and 25% of the total soil area respectively (Tian *et al.*, 2017). Xiangjiang River is the main river of Changsha and there are 15 tributaries flowing into it, including Liuyang River, Laodao River, Jinjiang River and so on. There are abundant water resources. Water does not freeze in winter and contains little sand (Tian *et al.*, 2018).

Training data creation and remote sensing imagery acquisition. The boundary of Changsha is acquired from open source GADM data. (n.d.) which contains World countries boundary as a vector ESRI shp files. Given the large area of Changsha city a big size of training data is required to achieve a satisfied classification accuracy. Firstly, the systematic sampling design was carried out within the official Changsha city boundary which includes most common land cover types, and the distance between each sampling point is set as 10x10 km. For each year of observation, authors have created 106 polygons (as a buffer around each sampling point) with 5 cover classes: cropland, forest, open soil or bare land, settlement areas, and water bodies. Using the designed network of sampling points the training polygons of different land cover types were drawn in Google Earth Pro software using time slider tool in order to select the background imagery for the indicated time (year). Using zooming tool, authors carefully analysed land cover types and drawn training polygons. Given that, it was prepared the dataset of training polygons for each year of study that cover a considerably big number of pixels as follows: 2005 – 15631 pixels; 2010 – 16345 pixels, 2015 – 14765 pixels; and 2020 – 18851 pixels respectively. The minimum number of pixels (856) were observed for the smallest land cover class – open soil or bare land, the rest of classes were represented with the more than 1000 reference pixels. The generated reference polygons were converted into vector layer then imported into Google Earth Engine platform and ArcGIS software for further analysis.

There are various classification standards of LULC types, such as the criteria provided by United Nations, Natural Resources Defense Council (NRDC), U.S. Geological Survey (USGS) and so on. For our study the main purpose was to locate the land cover changes especially settlement areas, woodlands and croplands, the five-fold LULC class system was selected with the following classes:

- *Cropland.* Cropland includes most flat areas and some steep slopes where a variety of food crops and some low height grass vegetation are grown, either feed on rainwater or irrigation. In Changsha, irrigation is a common practice, because there are significant seasonal differences in rainfall, mainly in the spring.
- *Forest.* Forest is the area dominated by woody plants, also including other plants, animals, microorganisms. It has abundant species, complex structure and various functions. The shrublands has been also included into this land cover category.
- *Open soil and bare land* (also named as *"Other land"* in this manuscript). Other land mainly includes bare land (it is not covered by any crop, grass or any other shrub or tree species, mainly including exposed sand, salt flats and exposed rock or cleared territories before construction process. (WBISPP, 2002).
- *Settlements.* It is a large residential area formed by non-agricultural industry and non-agricultural population agglomeration, usually have a dense population. This category

includes both urban land and rural settlements (Esetlili & Sunar, 2017).

◈ *Water bodies.* It is the general term for the liquid that forms the surface of the earth in nature. It includes rivers, oceans, glaciers, lakes, marshes, and other surface water bodies. The water cover type in Changsha is represented mainly in the form of rivers, irrigation canals, and lakes.

Based on this classification scheme, the training polygons have been created. It should be noticeable the number of polygons in a class must be corresponding to the real area of that class, which means that the larger the area, the more polygons are taken in the class, and vice versa. The size of each polygon was chosen with the assumption that each polygon must cover at least 10 pixels of Landsat image (30x30 m). Polygons should be a convex shape, not a concave one. Also, polygons should be drawn in the middle of the class, as far as possible away from edge to avoid possible confusions during training the classifier procedure.

Compilation of the remote sensing data was performed using the Google Earth Engine API (GEE). GEE uses state-of-the-art cloud-computing and storage capabilities that have been archived in a large catalogue of earth observation data. It is highly efficient to work on petabytes of satellite imagery rapidly using parallel cloud computing on the Google servers. GEE platform works on JavaScript programming language. Most importantly, using GEE it was possible to develop our own script which allowed us to apply all the necessary filters and prepare yearly Landsat image mosaics with the median values of reflectance. Another important advantage of the use of GEE was the possibility to select already corrected Landsat images. Using specifically developed algorithm all Landsat images went through radiometric and top of atmosphere (TOA) corrections (Midekisa *et al.*, 2017).

In this study Landsat 7 was used for Changsha city land cover classification in 2005 and 2010; Landsat 8 was used in 2015 and 2020 respectively. Landsat satellite data, that were used in this research, are free available satellite imageries with both moderate spatial and spectral resolution without clouds. The Landsat-8 satellite payload consists of two science instruments –the Operational Land Imager (OLI) and the Thermal Infrared Sensor (TIRS). These two sensors provide seasonal coverage of the global landmass at a spatial resolution of 30 meters (visible, NIR, SWIR); 100 meters (thermal); and 15 meters (panchromatic). TIRS images consist of nine spectral bands with a spatial resolution of 30 meters for Bands 1 to 7 and 9. New band 1 (ultra-blue) is useful for coastal and aerosol studies. New band 9 is useful for cirrus cloud detection (Mateo-García *et al.*, 2018). The resolution for Band 8 (panchromatic) is 15 meters. Thermal bands 10 and 11 are useful in providing more accurate surface temperatures and are collected at 100 meters (Irene *et al.*, 2017). The images in this study were taken in 2005 (Landsat 7), 2010 (Landsat 7), 2015 (Landsat 8), and 2020 (Landsat 8) respectively.

To get more cloud-free images, the starting and ending times are set to be two months before and two months after the target year. After that, another filter was applied based on cloud score (percentage of cloud cover on the image). In this case images with cloud score less than 5% were selected and ranked by the principle: lowest cloud cover on top and biggest – on the bottom. Finally, to get yearly image composite authors used median value of every pixel of study area out of the selected images set. The only 30 m resolution spectral bands and some simple band ratios of Landsat images have been selected for the future classification. For the Landsat 8 authors used near infrared (NIR) and thermal bands: Band 2 (0.45-0.52 μm), Band 3 (0.525-0.60 μm), Band 4 (0,64-0,67 μm), Band 5

(0,85-0,88 μm), Band 6 (1,57-1,65 μm), Band 7 (2,11-2,29 μm), Band 10 (10,60-11,19 μm), Band 11 (11,50-12,51 μm) as well as band ratio recommended by V. Myroniuk *et al.* (2020) as follows: Band 4 / Band 5, Band 4 / Band 7, Band 5 / Band 7. Finally, the NDVI index.

As a result, the whole year image composite has been created with 11 bands ready for the classification, based on Landsat Image time series. The same approach was applied for each target year.

***Random Forest classifier settings*.** The programming script in GEE environment has been developed by authors and run Random Forest algorithm for the classification of study area using training polygons and Landsat yearly composites for each target year 2005, 2010, 2015 and 2020 accordingly. Basic settings of RF classifier were as follows: number of decision trees: 500; OBB mode used; fraction of data for each iteration: 67%; portion of training data for error estimation: 33%; number of variables per split in every node: 11.

Using the training datasets, authors performed firstly the training accuracy estimation of the classifier for each year. It has been obtained more than 97% overall training accuracy of the RF classification based on the reference pixels. Having satisfied results of training overall accuracy it was concluded that the RF classifier is ready for the classification of the entire study area. After the conducting the classification procedure in GEE environment, 4 raster classified raster images of Changsha city for the target observation years have been produced and then exported these rasters into ArcGIS software for further analysis.

The next step was accuracy assessment of the obtained raster land cover maps of Changsha city at the indicated years. To do this, it is needed to evaluate the differences between classified data and ground truth data (accurate data), which helps users to know if the data is reliable or not (Stehman & Czaplewski, 1998). In this study, authors analysed the LULC changes of Changsha which is quite big area. Hence, gathering of field references data using GPS or aerial photos is time consuming and expensive, therefore choose multiple resolution imagery and Google Earth software were used. Simple random sampling method was utilized for preparing the network of validation points. The total number of points is dependent on the number of classes and sampling strategy. According to the standard principle that the minimum required number has to be no less than 50 points in each land cover class. In our case, having 5 classes, at least 250 validation points should be created. As the area of interest is constant, the number of random points is proportional to the area of the corresponding class. Due to the small coverage of some categories such as bare land and water, the points covered by them are likely to be less than 50. Hence, there were more than 500 random points created for each year. A standard accuracy assessment procedure was applied by authors that requires construction of error matrix, calculation of User's, Producer's, Overall accuracy percentage, and Kappa statistics (Rwanga & Ndambuki, 2017).

Results

***Changsha city land cover classified raster maps*.** Using ArcGIS 10.5 software and classified Landsat image composites previously prepared in GEE by the described above approach, four continuous thematic land cover raster maps have been produced of Changsha for year 2005, 2010, 2015 and 2020. The mapping results are shown on the Figure 2.

Form the Figure 2, the Changsha urbanized area was divided into two parts along the Xiangjiang River. The left riverbank mostly represented as farmlands and the right – mostly forests. The highest density of buildings is

mainly concentrated in the middle of study area along the Xiangjiang River. From 2005 to 2010, the urban area expanded further along Xiangjiang riverbanks where urban settlements of Changsha originated. However, the area of forests was taken by urban area and cropland as the total area of Changsha did not change. From 2010 to 2015, the newly increased urban spots were scattered across the study area which is usually described as 'patches' in landscape field. The forest area increased slightly during that period. From 2015 to 2020, some patches of settlements became interconnected. At the same time, the size of patches doubled at cropland area's expense. The overall layout of Changsha showed that based on the settlement center around Xiangjiang River, small settlements spread out within the study boundary.

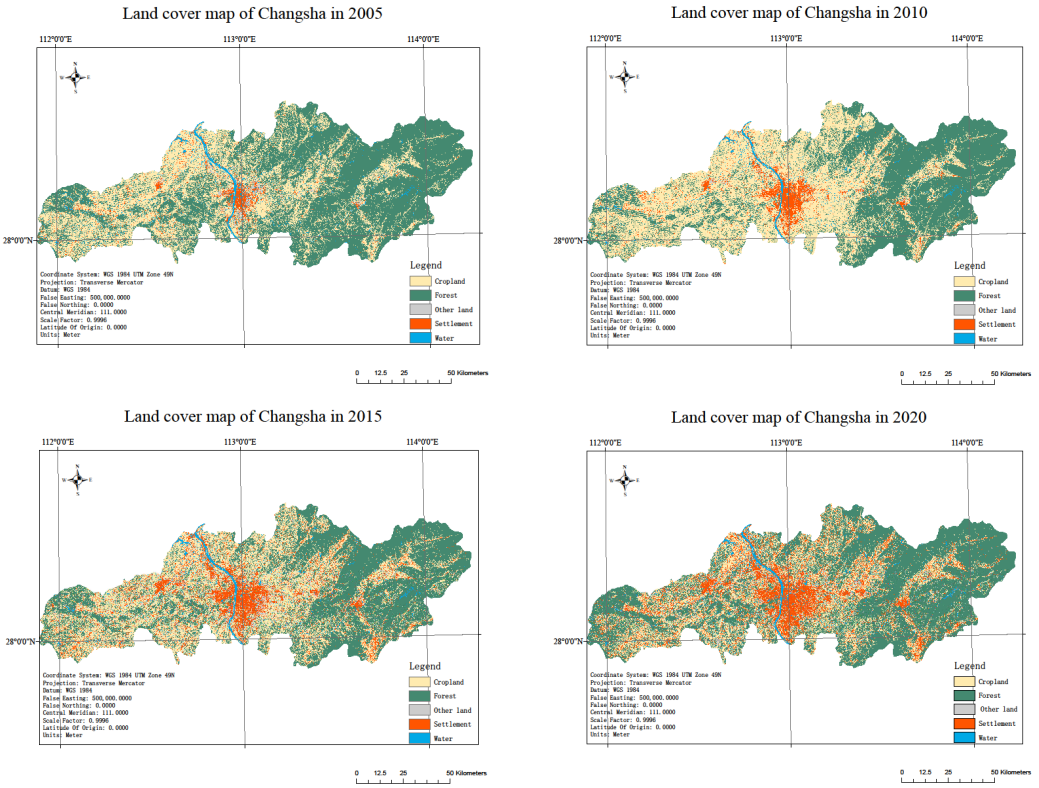

Figure 2. The classified land cover raster maps of Changsha city in 2005, 2010, 2015, and 2020
Source: developed by the authors

With the aim to check the accuracy of the obtained results, authors used common approach which based on the preparation of the sets of reference points, creation error matrix and calculate User's, Producer's and Overall accuracies and finally, Kappa statistics.

Accuracy assessment of the classification results. The of the accuracy assessment have been performed according to the described above procedure. The error matrix was created based on the sets of specifically created validation points for each year of observation

(500 point for each year). The overall accuracy, as well as User's and Producer's accuracies and Kappa statistics are provided in the Table 1.

The overall accuracy in 2020, 2015, 2010 and 2005 are 85.13%, 86.09%, 87.15% and 83.80% respectively. The Kappa coefficient is 0.84 and higher, which approves high level of the classification results. The producer's accuracy of forestland cover type and water bodies demonstrated the highest levels of accuracy (90% or higher) compared with the other classes. It can point out that User's accuracy commonly has higher values than Producer's. The settlements cover class identification has also shown satisfied levels of both Producer's and user's accuracies (close to 80% and higher.

Table 1. The accuracy calculation results for the produced land cover maps of Changsha city

Year of observation		2020	2015	2010	2005
Overall Acc, %		85.13	86.09	87.15	83.80
Kappa coefficient		0.84	0.85	0.86	0.84
Producer's Accuracy, %	Cropland	88.24	90.74	92.62	84.92
	Forest	92.91	95.05	89.80	94.69
	Other land	88.46	77.97	76.56	76.10
	Settlements	77.92	84.85	80.28	76.00
	Water	97.50	83.87	94.83	88.14
User's Accuracy, %	Cropland	85.29	75.38	83.09	82.31
	Forest	89.37	90.57	92.31	86.29
	Other land	88.46	88.00	81.67	75.00
	Settlements	80.00	78.87	86.36	81.43
	Water	91.76	98.11	96.49	92.86

Source: developed by the authors

Changsha city land cover change dynamics during the period 2005 to 2020. According to the obtained land cover raster maps of Changsha city the proportion of each land cover type in different years is calculated in ArcGIS software and expressed in the form of percentage in year 2005, 2010, 2015 and 2020 (Fig. 3).

During the period 2005-2020, the percentage of forest is the highest (almost half a pie in each year) except for that in 2010. The proportion of cropland is closed to 36% in both year of 2005 and 2015. In 2010, it reaches the top with almost 50% of total area. The proportion of water bodies have not been changes significantly and it always shows a small percent about 3% only. The proportion of other (open soil and bare land) land cover class is the lowest among the five types during the whole study period. It takes up around 5.5% in 2010, which is the highest one. The proportion of urban area has been increased exponentially from 3.23% in 2005 to 15.95% in 2020.

The dynamics of urban (settlements cover type) area for the study period in absolute units (km^2) are shown on the Figure 4.

In general, the area of settlement has increased during the 15-year period from 380.4363 km^2 to 1880.1756 km^2 (1499.7393 km^2 totally increase). The area of forests decreases gradually from 2005 to 2015, however there is an increasing trend during 2015-2020, from 5281 to 6089 km^2 respectively. Figure 4 shows that from year 2005 to 2010, there is an increase of the area from 4239 to 5527 km^2, and then during the following ten years, it decreases to 3230 km^2 only. As for the open soil and other bare land cover, it fluctuates between 180 and

400 km². The highest area observed in 2015 (398 km²) which can be explained as a high intensity of contraction process at that period. Analysis of the water cover change shows that the change is generally small. The minimum value of 267 km² was obtained in 2010 and a peak of 392 km² in 2020. This can be explained as the development of irrigation canals and water reservoirs within the city when doing landscape design of the new residential areas.

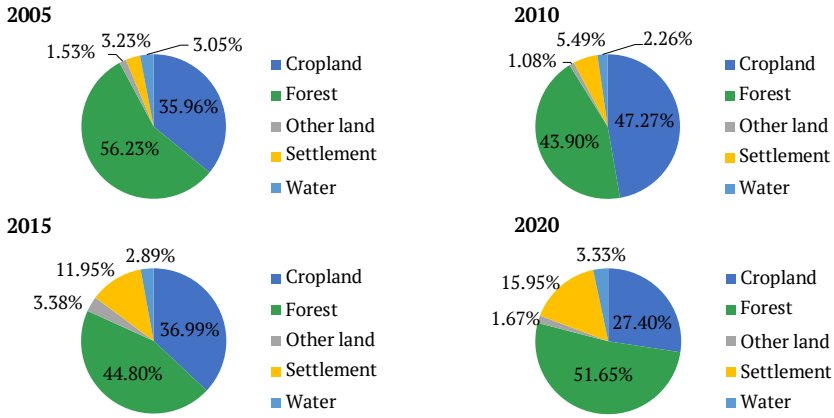

Figure 3. The percentage of different land cover types of Changsha city for the four observation years (2005, 2010, 2015, and 2020)

Source: developed by the authors

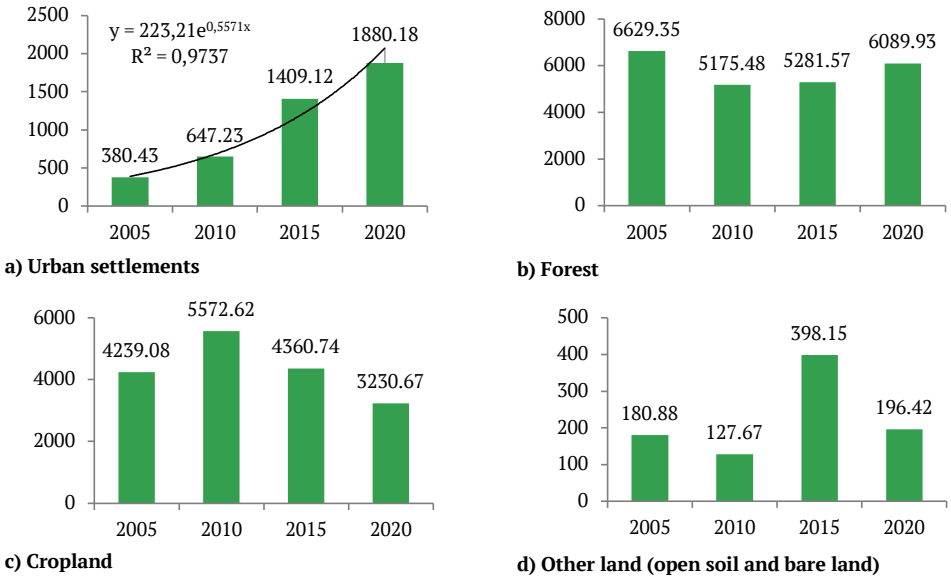

Figure 4. The dynamic change of the main land cover types (in km²) of Changsha city in 2005-2020

Source: developed by the authors

The analysis of factors that may cause an impact on Changsha urban areas expansion.
Natural environment is the basic restriction condition of urban space expansion. Changsha city is located in the transition zone from hills to plains, so the landform of this range is diversified. Specifically, the west side of the city is low mountainous area, the northeast side is granite low hilly area, the north part has dense and developed river network, the south is low hilly area and only the middle part is flat terrain. Considering of the cost of urban constructions, the input of infrastructure in the plain area is significantly lower than that in the hill area and it is easy to arrange industrial projects and residential areas, which determines that the urban construction of Changsha takes the Xiangjiang River as the central axis and presents a north-south urban development pattern. Due to the restriction of mountain barriers and water system division, the city cannot spread continuously like cities with flat terrain.

Economic development, transportation development and population growth. The growth of urban population and economy is the basic power of urban land expansion. On the one hand, the growth of urban economy itself needs more land as support. On the other hand, the rural-shift to-urban population increases urban load-bearing pressure. In addition, the neglect of the old city reconstruction has made the problem of urban land extension faster. Some research studies show that the distribution of traffic network and urban settlements has a linear relationship (Poumanyvong *et al.*, 2012). In recent years, Changsha High-speed Railway station (2009), Changsha Metro (2014), Changsha-Zhuzhou-Xiangtan Intercity Railway (2017) were constructed and operated on a regular basis, which provides the urban industries and companies nearby with a wide accessibility to various destinations (Kotavaara, Antikainen and Rusanen, 2011), therefore population increased as much employment was provided.

Planning policies of urban areas development and design. According to urban planning policies of Changsha government, 2500 km^2 area adjacent to the core development area of Changsha is planned as ecological protection zone and urban constructions are forbidden there that helps to protect the forested areas efficiently. Urban underground spaces should be developed to reduce the occupation of new urban land, therefore protecting farmland areas, and other local regulations.

This study with the proposed LULC mapping approach might be useful for solving various important tasks related to the continuous monitoring of the land cover changes. This may become a basis for the ecosystem service valuation procedures and might help the Changsha government and decision makers to support a sustainable city land use planning in order to receive economic benefits as well as valuable ecosystem services. The conducted research helps to control the increase rate of settlement land category strictly and make great focus on conservation and increase the areas of woodland and water body which could provide a greater level of ecosystem services.

Discussion

Similar studies that were based on the use of RF classifier and Landsat time-series imagery demonstrated close results of accuracy assessment comparing to ours. For example, the land cover map of Changsha City using Landsat 8 datasets and pixel-based method classification approach published by Z. Deng *et al.* (2019) demonstrated 88.62% of overall accuracy and 0.83 Kappa coefficient. The overall classification accuracy using Landsat 8 OLI data with feature selection reached 82% in a case study of land cover mapping in Yunnan Province, China (Pan *et al.*, 2022). Another land cover map produced for the eastern edge of the Tibetan Plateau in the north of Sichuan Province, China

(Zhu, 2013) showed overall accuracy of the 82% with a Kappa coefficient of agreement of 0.73. Therefore, it can be stated that the prepared training dataset size in combination with the suggested Landsat time series image composite as well as proper RF classifier settings demonstrated reliable classification results.

The effectiveness of RF algorithm and Landsat time-series data to analyse land use and land cover change have been investigated by S. Amini *et al*. (2022). The impact of different image compositions and auxiliary data, such as digital elevation model (DEM) and land surface temperature (LST), on final classification accuracy was also explored. The proposed algorithm achieved high accuracy levels, with an overall accuracy of 94.438%, Kappa of 0.93. The algorithm's success in obtaining high accuracies indicates its potential for efficient extraction of spatiotemporal information for LULC classification. The three LULC maps have been created for 2010, 2015, and 2020 in Rahuri watershed area, India using the google earth engine and RF classifier (Pande, 2022). Similar to our study, the entire three years of land use and land cover produced high accuracy (OA ranges from 85.53% to 94.34%). Agriculture and built-up land were divided with the greatest precision, followed by forest and other land. The author approves that GEE is a successful platform for accessing and processing satellite data through the use of various classification algorithms in combination with geographic object-oriented or pixel-based analysis techniques. The study conducted by G. Ge *et al.* (2020) compares the performances of four most popular machine learning algorithms in classifying land use and cover change in the Dengkou Oasis region of China using Landsat-8 OLI image data. The study finds that artificial neural networks has the highest overall accuracy (97.16%), followed by RF (96.92%), SVM (96.20%), and KNN (93.98%). RF is recommended as a good first choice method for land-cover classification in this study area.

J. Cui *et al.* (2022) investigated land use/land cover changes and their driving factors in the Yellow River Basin of Shandong Province, China, using Google Earth Engine from 2000 to 2020. The results showed that the main changes in land use/land cover were the increase in construction land and decrease in cultivated land, woodland, and grassland. The overall accuracy exceeded 86% indicating that the classification results were reasonable and reliable. The changes were primarily driven by population growth, economic development, and urbanization. The Random Forest classifier was found to be an effective method for mapping land use/land cover in the study area.

S. Feng *et al*. (2022) utilized the Google Earth Engine (GEE) platform to conduct land use classification in a large area with a complex workflow, achieving fast and accurate results. The pixel-based Random Forest (RF) classification method was used for land use classification, which yielded overall accuracy above 87% and kappa coefficient 0.88 that met the requirements. However, due to the absence of object-oriented thinking, the method produced some salt and pepper noise that is similar to our study. Therefore, future research should focus on the integration of image segmentation and feature matching to improve the land use classification method in the study area. The RF algorithm demonstrated potential to work with various datasets, high-dimensional data, and interaction between features during training, while having a fast training pace and low computing cost. RF showed a minimum accuracy of 79.54% in a study conducted by B. Feizizadeh *et al.* (2023). It confirms decent performance with minimal tendency to overfit and has been applied to various applications such as landslide susceptibility mapping, sustainability assessment, and landform mapping.

The results of our study indicates that the use of LULC maps and change detection based on them are recognized as valuable for various applications, including land use planning and allocation, environmental impact analysis, and assessment of sustainable development. The outcome of this research can be essential for decision makers and authorities in local governmental departments and stakeholders to observe the environmental issues of the Changsha city in the next decades.

Conclusions

In this paper, a comprehensive approach of land use/cover mapping was enriched. The described method demonstrates the potential possibilities of the use Landsat time-series image composites and RF classifier for the LULC mapping and monitoring changes for the Changsha city study area. GEE platform provides a wide range of abilities to search, filter and process of a huge amounts and types of spatial-temporal remote sensing data. The produced continuous land cover raster maps of Changsha city enable us to do the monitoring of land cover change dynamic for the period 2005-2020. From 2005 to 2020, the proportion of urban area has been gradually increased from 3.23% to 15.95% and the area has increased by 1500 km^2. However, the area of cropland has declined by 1008 km^2, however, forestland class shows a growth trend at the latest 5 years observation period. The accuracy assessment result allows us to make a conclusion that chosen approach can be successfully used for solving tasks related to classification and monitoring of city land cover changes. Further research could focus on the integration of additional data sources, such as high-resolution imagery and LiDAR data, and classification algorithms for better identification of different land cover types and more accurate mapping of urban areas.

Conflict of Interest

The authors declare no conflict of interest.

Acknowledgements

The authors would like to thank the Google Earth Engine developers for providing the open access to the cloud computing facilities that helped as to conduct our experiment.

References

[1] Amini, S., Saber, M., Rabiei-Dastjerdi, H., & Homayouni, S. (2022). Urban land use and land cover change analysis using random forest classification of Landsat time series. *Remote Sensing*, 14(11), article number 2654. doi: 10.3390/rs14112654.

[2] Ayanu, Y., Conrad, C., Jentsch, A., & Koellner, T. (2015). Correction: Unveiling undercover cropland inside forests using landscape variables: A supplement to remote sensing image classification. *PLoS ONE,* 10(8), article number e0137150. doi: 10.1371/journal.pone.0137150.

[3] Banerjee, B., & Buddhiraju, K. (2015). A novel semi-supervised land cover classification technique of remotely sensed images. *Journal of the Indian Society of Remote Sensing. New Delhi: Springer India,* 43(4), 719-728. doi: 10.1007/s12524-014-0370-z.

[4] Batty, M. (2008). The size, scale, and shape of cities. *Science. American Association for the Advancement of Science*, 319(5864), 769-771. doi: 10.1126/science.1151419.

[5] Breiman, L. (2001). Random forests. *Machine Learning,* 45, 5-32. doi: 10.1023/A:1010933404324.

[6] Chaolin, G., Liya, W., & Cook, I. (2012). Progress in research on Chinese urbanization. *Frontiers of Architectural Research*, 1(2), 101-149. doi: 10.1016/j.foar.2012.02.013.

[7] Chen, X., Yu, B., Zhou, D., Zhou, W., Gong, J., Li, S., & Stanton, B. (2015) A comparison of the number of men who have sex with men among rural-to-urban migrants with non-migrant rural and urban residents in Wuhan, China: A GIS/GPS-assisted random sample survey study. *PLoS ONE*, 10(8), article number e0134712. doi: 10.1371/journal.pone.0134712.

[8] Corona, P. (2010). Integration of forest mapping and inventory to support forest management. *IForest – Biogeosciences and Forestry*, 3(3), 59-64. doi: 10.3832/IFOR0531-003.

[9] Cui, J., Zhu, M., Liang, Y., Qin, G., Li, J., & Liu, Y. (2022). Land use/land cover change and their driving factors in the Yellow River Basin of Shandong Province based on Google Earth Engine from 2000 to 2020. *ISPRS International Journal of Geo-Information*, 11(3), article number 163. doi: 10.3390/ijgi11030163.

[10] Deng, Z., Zhu, X., He, Q., & Tang, L. (2019). Land use/land cover classification using time series Landsat 8 images in a heavily urbanized area, *Advances in Space Research*, 63(7), 2144-2154. doi 10.1016/j.asr.2018.12.005.

[11] Eisavi, V., Homayouni, S., Yazdi, A.M., & Alimohammadi, A. (2015). Land cover mapping based on random forest classification of multitemporal spectral and thermal images. *Environmental Monitoring and Assessment*, 187, 1-14. doi: 10.1007/s10661-015-4489-3.

[12] Esetlili, M., & Sunar, F. (2017). Evaluation of image fusion methods using PALSAR, RADARSAT-1 and SPOT images for land use/ land cover classification. *Journal of the Indian Society of Remote Sensing. Dordrecht: Springer Science & Business Media*, 45(4), 591-601. doi: 10.1007/s12524-016-0625-y.

[13] Feizizadeh, B., Omarzadeh, D., Garajeh, M. K., Lakes, T., & Blaschke, T. (2023). Machine learning data-driven approaches for land use/cover mapping and trend analysis using Google Earth Engine. *Journal of Environmental Planning and Management*, 66(3), 665-697. doi: 10.1080/09640568.2021.2001317.

[14] Feng, L., Chen, B., Hayat, T., Alsaedi, A., & Ahmad, B. (2017). The driving force of water footprint under the rapid urbanization process: a structural decomposition analysis for Zhangye city in China. *Journal of Cleaner Production. Elsevier Ltd*, 163(S), S322-S328. doi: 10.1016/j.jclepro.2015.09.047.

[15] Feng, S., Li, W., Xu, J., Liang, T., Ma, X., Wang, W., & Yu, H. (2022). Land use/land cover mapping based on GEE for the monitoring of changes in ecosystem types in the upper Yellow River Basin over the Tibetan Plateau. *Remote Sensing*, 14(21), article number 5361. doi: 10.3390/rs14215361.

[16] Firpi, O.A.A. (2016). Satellite data for all? Review of Google Earth Engine for archaeological remote sensing. *Internet Archaeology. University of York,* 42. doi: 10.11141/ia.42.10.

[17] Friedmann, J. (2003). China's Urbanization. *International Journal of Urban and Regional Research*, 27(3), 745-758. doi: 10.1111/1468-2427.00480.

[18] Friedmann, J. (2011). Becoming urban: Periurban dynamics in Vietnam and China – introduction. *Pacific Affairs*, 84(3), 425-434. doi: 10.5509/2011843425.

[19] GADM data. (n.d.). Retrieved from https://gadm.org/data.html.

[20] Ge, G., Shi, Z., Zhu, Y., Yang, X., & Hao, Y. (2020). Land use/cover classification in an arid desert-oasis mosaic landscape of China using remote sensed imagery: Performance assessment of four machine learning algorithms. *Global Ecology and Conservation*, 22, article number e00971. doi: 10.1016/j.gecco.2020.e00971.

[21] He, C., Zhanga, D., Huanga, Q., & Zhao, Y. (2016). Assessing the potential impacts of urban expansion on regional carbon storage by linking the LUSD-urban and InVEST models. *Environmental Modelling and Software*, 75, 44-58. doi: 10.1016/j.envsoft.2015.09.015.

[22] Martinez, H.M., & Cartier, C. (2017). City as province in China: The territorial urbanization of Chongqing. *Eurasian Geography and Economics. Routledge*, 58(2), 201-230. doi: 10.1080/15387216.2017.1312474.

[23] Jin, M., Dickinson, R., & Zhang, D. (2005). The footprint of urban areas on global climate as characterized by MODIS. *Journal of Climate*, 18(10), 1551-1565. doi: 10.1175/JCLI3334.1.

[24] Kolotii, A., Kussul, N., Shelestov, A., Skakun, S., Yailymov, B., Basarab, R., Lavreniuk, M., Oliinyk, T., & Ostapenko, V. (2015). Comparison of biophysical and satellite predictors for wheat yield forecasting in Ukraine. *ISPRS*, XL-7/W3, 39-44. doi: 10.5194/isprsarchives-XL-7-W3-39-2015.

[25] Kutia, M., Myroniuk, V., & Sarkissian, A. (2018). Evaluation of Sentinel-2 composited mosaics and random forest method for tree species distribution mapping in suburban areas of Kyiv City, Ukraine. In *Proceedings of the International Workshop on Environmental Management, Science and Engineering – IWEMSE* (pp. 597-604). Xiamen, China. doi: 10.5220/0007563505970604.

[26] Lambin, E.F., Turner, B.L., Geist, H.J., Agbola, S.B., Angelsen, A., Bruce, J.W., Coomes, O.T., Dirzo, R., Fischer, G., Folke, C., George, P.S., Homewood, K., Imbernon, J., Leemans, R., Li, X., Moran, E.F., Mortimore, M., Ramakrishnan, P.S., Richards, J.F., Skånes, H., Steffen, W., Stone, G.D., Svedin, U., Veldkamp, T.A., Vogel, C., & Xu, J. (2001). The causes of land-use and land-cover change: Moving beyond the myths. *Global Environmental Change,* 11(4), 261-269. doi: 10.1016/S0959-3780(01)00007-3.

[27] Li, H., Huang, X., Kwan, M.-P., Bao, H.X.H., & Jefferson, S. (2015). Changes in farmers' welfare from land requisition in the process of rapid urbanization. *Land Use Policy*, 42, 635-641. doi: 10.1016/J.LANDUSEPOL.2014.09.014.

[28] Lin, B.B., Egerer, M.H., Liere, H., Jha, Sh., Bichier, P., & Philpott, S.M. (2018). Local- and landscape-scale land cover affects microclimate and water use in urban gardens. *Science of the Total Environment*, 610-611, 570-575. doi: 10.1016/j.scitotenv.2017.08.091.

[29] Liu, Y., Zuo, R., & Dong, Y. (2021). Analysis of temporal and spatial characteristics of urban expansion in Xiaonan district from 1990 to 2020 using time series Landsat imagery. *Remote Sensing*, 13(21), article number 4299. doi: 10.3390/rs13214299.

[30] Luo, S., & Yan, W. (2018). Evolution and driving force analysis of ecosystem service values in Guangxi Beibu gulf coastal areas, China. *Acta Ecologica Sinica,* 9, article number 3248. doi: 10.5846/stxb201704050578.

[31] Ma, Y., Wu, H., Wang, L., Huang, B., Ranjan, R., Zomaya, A.Y., & Jie, W. (2015). Remote sensing big data computing: Challenges and opportunities. *Future Generation Computer Systems*, 51, 47-60. doi: 10.1016/j.future.2014.10.029.

[32] Mateo-García, G., Gómez-Chova, L., Amorós-López, J., Muñoz-Marí, J., & Camps-Valls, G. (2018). Multitemporal cloud masking in the Google Earth Engine. *Remote Sensing*, 10(7), article number 1079. doi: 10.3390/rs10071079.

[33] Miao, J., & Wu, X. (2016). Urbanization, socioeconomic status and health disparity in China. *Health & Place*, 42, 87-95. doi: 10.1016/j.healthplace.2016.09.008.

[34] Midekisa, A., Holl, F., Savory, D.J., Andrade-Pacheco, R., Gething, P.W., Bennett, A., Andrade-Pacheco, R., Gething, P., Bennett, A., & Sturrock, H. (2017). Mapping land cover change over continental Africa using Landsat and Google Earth Engine cloud computing. *PLoS ONE*, 12(9), article number e0184926. doi: 10.1371/journal.pone.0184926.

[35] Myroniuk, V., Kutia, M., Sarkissian, A.J., Bilous, A., & Liu, S. (2020). Regional-scale forest mapping over fragmented landscapes using global forest products and Landsat time series classification. *Remote Sensing*. 12(1), article number 187. doi: 10.3390/rs12010187.

[36] Pan, J., Wang, C., Wang, J., Gao, F., Liu, Q., Zhang, J., & Deng, Y. (2022). Land cover classification using ICESat-2 photon counting data and Landsat 8 OLI Data: A case study in Yunnan Province, China. *IEEE Geoscience and Remote Sensing Letters*, 19, article number 2507405. doi: 10.1109/LGRS.2022.3209725.

[37] Pande, C.B. (2022). Land use/land cover and change detection mapping in Rahuri watershed area (MS), India using the google earth engine and machine learning approach. *Geocarto International,* 37(26), 13860-13880. doi: 10.1080/10106049.2022.2086622.

[38] Poumanyvong, P., Kaneko, S., & Dhakal, S. (2012). Impacts of urbanization on national transport and road energy use: Evidence from low, middle and high income countries. *Energy Policy,* 46, 268-277. doi: 10.1016/J.ENPOL.2012.03.059.

[39] Puletti, N., Perria, R., & Storchi, P. (2014). Unsupervised classification of very high remotely sensed images for grapevine rows detection. *European Journal of Remote Sensing*, 47, 45-54. doi: 10.5721/EuJRS20144704.

[40] Roy, D.P., Wulder, M.A., Loveland, T.R., Woodcock, C.E., Allen, R.G., Anderson, M.C., Helder, D., Irons, J.R., Johnson, D.M., Kennedy R., Scambos, T.A., Schaaf, C.B., Schott, J.R., Sheng, Y., Vermote, E.F., Belward, A.S., Bindschadler, R., Cohen, W.B., Gao, F., Hipple, J.D., Hostert, P., Huntington, J., Justice, C.O., Kilic, A., Kovalskyy, V., Lee, Z.P., Lymburner, L., Masek, J.G., McCorkel, J., Shuai, Y., Trezza, R., Vogelmann, J., Wynne, R.H., & Zhu, Z. (2014). Landsat-8: Science and product vision for terrestrial global change research. *Remote Sensing of Environment*, 145, 154-172. doi: 10.1016/J.RSE.2014.02.001.

[41] Rwanga, S., & Ndambuki, J. (2017). Accuracy assessment of land use/land cover classification using remote sensing and GIS. *International Journal of Geosciences,* 8, 611-622. doi: 10.4236/ijg.2017.84033.

[42] Seto, K.C., Kaufmann, R.K., & Woodcock, C.E. (2000). Landsat reveals China's farmland reserves, but they're vanishing fast. *Nature,* 406(6792), article number 121. doi: 10.1038/35018267.

[43] Song, W., & Deng, X. (2017). Land-use/land-cover change and ecosystem service provision in China. *Science of The Total Environment*, 576, 705-719. doi: 10.1016/J.SCITOTENV.2016.07.078.

[44] Stehman, S.V., & Czaplewski, R.L. (1998). Design and analysis for thematic map accuracy assessment: Fundamental principles. *Remote Sensing of Environment,* 64, 331-344. doi: 10.1016/S0034-4257(98)00010-8.

[45] Su, S., Jiang, Z., Zhang, Q., & Zhang, Y. (2011). Transformation of agricultural landscapes under rapid urbanization: A threat to sustainability in Hang-Jia-Hu region, China. *Applied Geography*, 31(2), 439-449. doi: 10.1016/j.apgeog.2010.10.008.

[46] Tian, K., Huang, B., Xing, Z., & Hu, W. (2017). Geochemical baseline establishment and ecological risk evaluation of heavy metals in greenhouse soils from Dongtai, China, *Ecological Indicators,* 72, 510-520. doi: 10.1016/j.ecolind.2016.08.037.

[47] Tian, Y., Xu, Y.P., & Wang, G. (2018). Agricultural drought prediction using climate indices based on Support Vector Regression in Xiangjiang River basin. *The Science of the Total Environment*, 622-623, 710-720. doi: 10.1016/j.scitotenv.2017.12.025.

[48] Tse-Tung, M. (2017). Changsha. *Literary Review. Madison: Fairleigh Dickinson University*, 60(3), 24-295.

[49] Welch, R., Pannell, C.W., & Lo, C.P. (1975). Land use in Northeast China, 1973: A view from Landsat-1. *Annals of the Association of American Geographers,* 65, 595-596. doi: 10.1111/j.1467-8306.1975.tb01067.x.

[50] Yan, Y., Ju, H., Zhang, S., & Jiang, W. (2020). Spatiotemporal patterns and driving forces of urban expansion in coastal areas: A study on urban agglomeration in the Pearl River Delta, China. *Sustainability*, 12(1), article number 191. doi: 10.3390/su12010191.

[51] Yao, T., Zhang, X., Guan, H., Zhou, H., Hua, M., & Wang, X. (2018). Climatic and environmental controls on stable isotopes in atmospheric water vapor near the surface observed in Changsha, China. *Atmospheric Environment*, 189, 252-263. doi: 10.1016/j.atmosenv.2018.07.008.

[52] Zhang, J., Mauzerall, D.L., Zhu, T., Liang, S., Ezzati, M., & Remais, J.V. (2010). Environmental health in China: Progress towards clean air and safe water. *Lancet (London, England),* 375(9720), 1110-1119. doi: 10.1016/S0140-6736(10)60062-1.

[53] Zhou, G., & He, Y. (2007). The influencing factors of urban land expansion in Changsha. *Journal of Geographical Sciences,* 17, 487-499. doi: 10.1007/s11442-007-0487-x.

Класифікація земного покриву та моніторинг процесу урбанізації з використанням знімків Landsat на прикладі міста Чанша, провінція Хунань, Китай

Микола Миколайович Кутя
Доктор філософії, старший викладач
Бангорський коледж Китаю, Бангорський університет
410004, 498 Шаошан вул., м. Чанша, Китай
https://orcid.org/0000-0001-9996-2653

Дзіавей Лі
Студент магістратури
Саутгемптонський університет
SO17 1BJ, м. Саутгемптон, Велика Британія
https://orcid.org/0000-0002-3481-2942

Арбі Саркісян
Доктор філософії, викладач
Ланкастерський університет
LA1 4YW, м. Ланкастер, Велика Британія
https://orcid.org/0000-0003-4094-0884

Тім Паджелла
Старший викладач, доктор філософії
Бангорський університет,
LL57 2DG, м. Бангор, Велика Британія
https://orcid.org/0000-0001-5926-9299

Анотація. За прогнозами Організації Об'єднаних Націй, до 2050 року 64,1 % країн, що розвиваються, і 85,9 % розвинених країн будуть урбанізованими. Це призвело до швидких змін у землекористуванні та типах земного покриву на територіях навколо міст у всіх країнах, особливо в Китаї, що зумовлює актуальність цієї статті. Метою дослідження було оцінити динаміку змін рослинного покриву в місті Чанша, провінція Хунань, Китай, між 2005 і 2020 роками з використанням часових серій супутникових знімків Landsat і алгоритму класифікації Random Forest. Збір, попередня обробка та аналіз даних проводилися на загальнодоступній онлайн-платформі Google Earth Engine (GEE). Тематичні безперервні растрові карти рослинного покриву були створені за допомогою програмного забезпечення ESRI ArcGIS 10.5.1. Загальна точність класифікації склала понад 83 % для кожної створеної карти, а коефіцієнт Каппа – 0,84 і вище, що підтверджує достовірність результатів класифікації, які за отриманою точністю близькі до аналогічних нещодавніх досліджень. Дослідження показує, що з 2005 по 2020 рік площа густих поселень у місті Чанша, Китай, значно збільшилася, причому експоненціальне зростання міської території склало від 3,23 % до 15,95 %. Частка лісового покриву поступово зменшувалася з 2005 по

2015 рік, але збільшилася з 2015 по 2020 рік. Орні землі були другим найбільш домінуючим типом земельного покриву, з піком майже 50 % у 2010 році. Водні об'єкти залишалися стабільними на рівні близько 3 %. Частка відкритого ґрунту коливалася між 180 і 400 км2 (1,5-3 % від усієї площі). Дослідження показує, що запропонований підхід до моніторингу забезпечує надійні результати, а результати дослідження можуть бути використані для сталого міського планування та управління, а також для ініціатив зі збереження та розвитку. Дані дистанційного зондування та передові ГІС-технології можуть надати особам, які приймають рішення, точні дані для забезпечення сталого розвитку цієї території

Ключові слова: оцінка точності; алгоритм Random Forest; супутникові знімки; загальна точність; урбанізація